Iranian (Iranica) Journal of Energy & Environment
Journal Homepage: www.ijee.net
IJEE an official peer review journal of Babol Noshirvani University of Technology, ISSN:2079-2115

Thermal Performance and Heat Dynamics Energy and Exergy of Integrated Asphalt Collector Storage: Sources of Thermal Energy, and Thermoelectric Energy

M. Esmaeili Shayan[1,2]*, M. R. Hayati[1]

[1] *Department of Biosystem Engineering, Tarbiat Modares University, Tehran, Iran*
[2] *Saba Power and Energy Group, Tehran, Iran*

P A P E R I N F O

Paper history:
Received 05 August 2022
Accepted in revised form 28 August 2022

Keywords:
Asphalt road
Efficiency
Exergy
Renewable energy
Solar water heater

A B S T R A C T

Having kilometers of asphalt road, yet with this heat going to waste, an attempt has been made in this research to extract the road's renewable energy heat. The purpose of the experiment is to compare the energy and exergy efficiency of various materials of asphalt solar water heaters (ASWH), as well as heat transmission through the water tube and how friction affects exergy destruction. The water flow rate of one ASWH was 0.01 kg/s, while that of the other was 0.02 kg/s. Each ASWH has an area of 0.5 square meters. The copper tube is buried 10 mm deep in the asphalt. 15 degrees is the angle of inclination. The results indicate that the energy and exergy efficiencies are reasonably high for the water flow rate of 0.02 kg/s. Depending on the water flow rate, asphalt temperature, and sunlight intensity, the energy and exergy efficiencies changed from 32% to 65% and 5.8% to 16%, respectively. The water flow rate is an essential parameter for estimating the internal convective heat transfer coefficient and Reynolds number in order to calculate the friction factor in the copper tube based on internal convection heat transfer. In contrast, the friction factor is a consequence of the pressure loss and exergy degradation induced by friction.

doi: *10.5829/ijee.2023.14.01.03*

NOMENCLATURE

C_p	Specific heat	ECO	Economizer
$\dot{E}x$	Rate of exergy	EVAP	Evaporator
h	Enthalpy	FAR	Fuel air ratio
Q_{in}	Inlet heat	HLC	Hard line combustor
Q_{out}	Outlet heat	HRS	Heat recovery system
Q_{hr}	Heat released	ORC	Organic Rankine cycle
Q_w	Heat exchanged	RoHR	Rate of heat released
$\dot{m}$	Mass ratio	RoHC	Rate of heat capacity
$\dot{v}_a$	Actual volumetric air ratio	SLC	Soft line combustor
$\dot{v}_{as}$	Stoichiometric volumetric air ratio	WHR	Waste heat recovery
p	Pressure	**Greek symbol**	
P	Power	α	Stoichiometric ratio of carbon
v	Volume	β	Stoichiometric ratio of hydrogen
w	Work	φ	Equivalence ratio
Abbreviation		ρ	Density
CB	Carbon black	η	Efficiency
EPA	Environmental protection agency	γ	Stoichiometric ratio of oxygen

*Corresponding Author Email: mostafa.esmaeili@modares.ac.ir (M. Esmaeili Shayan)

Please cite this article as: M. Esmaeili Shayan, M. R. Hayati, 2023. Thermal Performance and Heat Dynamics Energy and Exergy of Integrated Asphalt Collector Storage: Sources of Thermal Energy, and Thermoelectric Energy, Iranian (Iranica) Journal of Energy and Environment, 14(1), pp. 17-25. Doi: 10.5829/ijee.2023.14.01.03

INTRODUCTION

The classic solar water heater is a flat-plate solar water heater (FP-SWH) (SWH). A FP-SWH is a basic system that collects and converts solar energy into heat using water as a heat transfer medium. It consists of a black absorber plate with a high thermal conductivity pipe, one or two transparent coverings a few millimeters above the absorber plate, well-insulated. FP-SWH performance analysis is a significant and important method for comprehending the system's overall performance. Numerous practical and theoretical investigations on the performance of FP-SWH have been thoroughly published by Attia et al. [1] and Rahmanian et al. [2]. Esmaeili Shayan et al. [3] reported on the experimental performance of a novel type of flat plate micro-heat pipe array solar water heater. Effective heat gain and thermal efficiency were employed to describe the performance. Annual daily effective heat gain and system efficiency were 9,5 MJ/m^2 and 58.29 percent, respectively. Also considered as a possible solar water heater shape was a cylindrical solar water heater [4]. Utilizing a cylindrical solar heater, researcher assessed the factors influencing the heater's performance, feces holding tank [5]. Some researchers studied the efficacy of a cylindrical solar water heater. It was made out of a cylindrical glass tube that served as a lid and a copper coil acting as the absorber surface. By the end of the experiment, the maximum efficiency was around 40% [6, 7].

Concrete-based collectors the design and integration of SWH into building components such as the roof and walls have been finished. On an inclined roof, Esmaeili Shayan et al. [10] studied and tested a concrete solar water heater (CSWH) for home hot water [8, 9]. A researcher installed a solar concrete collector on a flat roof to restrict a home's heat absorption while still supplying domestic hot water [10]. The parametric analysis and experimental and numerical research of a CSWH as integrated on the wall and/or facade were reported by Azadbakht et al. [11]. The objective of the study was to evaluate the efficiency of a concrete solar collector.

The asphalt solar collector (ASC) is a collector used to capture and convert solar energy [12]. Thermal performance of the mixed-asphalt solar water heater (MASWH) was investigated [13]. Meanwhile, the MASWH was utilized to integrate on the roof house in the same project, with the aim of minimizing heat input through the sloping roof. 5 to 12 W/m^2 of heat input into the home might be minimized [14]. The asphalt pavement functions as a solar collector. It has been investigated how asphalt pavement performs in terms of temperature, heat dynamics, and efficiency [14, 15].

The energy equation was utilized in the bulk of SWH research. In consequence, the exergy equation is crucial for modeling irreversible losses [17]. Esmaeili Shayan et al. [18] conducted an exergy analysis of domestic-scale solar water heaters (DSSWH). The objective of the initiative was to save money while preserving DSSWH's efficacy. A researcher published the exergy study of an integrated photovoltaic thermal solar water heater [16]. According to the research, the overall exergy and thermal efficiency of an integrated photovoltaic thermal solar system are greatest at a hot water withdrawal flow rate of 0.006 kg/s [19]. Afterwards, a researcher investigated the energetic and exergetic performance of integrated solar storage collectors. In the experiments, the energy and exergetic efficiencies were determined to be 32% and 23.5%, respectively [20]. The water temperature control equipment and solenoid valves were created. Under identical conditions, energy and exergy evaluations were conducted [21–23]. Azadbakht et al. [24] assessed the pipe designs of pavement solar collectors, which have been analyzed in terms of heat dynamics, performance, and system exergy.

This study examines the energy and exergy analyses, as well as the first and second law efficiencies, of the asphalt solar water heater (ASWH). Flow through the copper tube's internal convective heat transfer, pressure loss, and irreversibility will also be represented. Depending on the experimental measures, findings differ.

Experimental set-up and description

The asphalt solar water heaters (ASWH) utilized in this investigation were created. The research was conducted at Tehran, Iran. The experimental equipment utilized in this work is depicted in Figure 1. It consists of two asphalt solar water heaters of equal size.

The ASWH comprises a cover plate, an air gap, a copper tube, an absorber layer, and a well-insulated housing. A cover plate is a piece of glass with a 4 mm thickness. There is a 50 mm air gap between the cover glass and the absorber layer. A 50-millimeter-thick absorber layer was created using asphalt. A copper tube has an interior diameter of 9.52 mm, an exterior diameter of 10 mm, and a length of 8 m. The copper tube is encased

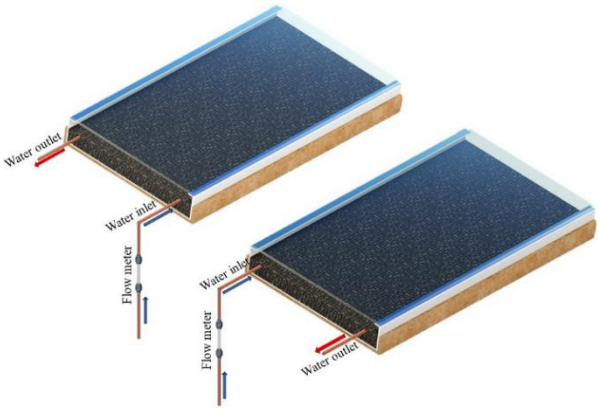

Figure 1. Experimental equipment schematic (Asphalt solar water heaters)

in asphalt 10 millimeters deep. The sides and rear of the ASWH were insulated with 10 mm of polyurethane insulation. Each ASWH is 1.0 m (0.5 m in size and 0.5 m2 in surface area. Depending on the flow meter, the water flow rates through copper tubes range from 0.01 to 0.02 kg/s. The inclination of ASWH was determined to be close to the local latitude (15 degrees, pointing south). Each absorber layer weighted around 30 kg.

The solar water heater is a heat exchanger that transmits heat at a consistent temperature from the collector to the water flow, or a single-stream heat exchanger. The copper tube is depicted in Figure 2(a), whereas the temperature profile is depicted in Figure 2(b).

Figure 3 illustrates the different ASWH measurement positions. The accuracy of Type K thermocouples is 5% across a temperature range of 0-1250°C. The top and bottom surfaces of a cover plate, the middle of the air gap, the absorber layer, the intake and exit of water flow, and the temperature of the ambient air were all measured (installed in an appropriate container). At three distinct depths, absorber layer measurements were taken (3 thermocouples at each depth). The thermocouples were specially calibrated for the testing. Total solar radiation was measured using a Kipp and Zonan CMP11 pyranometer with a range of 310 to 2800 meters and an uncertainty of 2%. Using a data logger with an accuracy of 0.8% (Hioki: Model-8422-51), temperature and solar radiation data were recorded. The water flow rate was controlled using calibrated flow meters (accuracy of 5%). The data from the experiment were recorded every 10 minutes. The trials were conducted in a real-world environment. Text should be created within the page dimensions displayed. Use the maximum permitted length with the two limitations listed below: I do not begin a new section at the bottom of a page; instead, relocate the heading to the top of the next column; (ii) you may only extend the length of the text area by one line to finish a section of text or a paragraph. You must use a line spacing of 1.0 (single) and the typeface Century Schoolbook. To avoid subscript and superscript fonts from overlapping and rendering your printed material unreadable, it is necessary to increase the space between text lines while inputting mathematically complex language. Ensure that your desktop publishing program's auto-adjust for interline spacing is set appropriately to prevent overlapping without leaving excessive gap.

(a) Copper tube

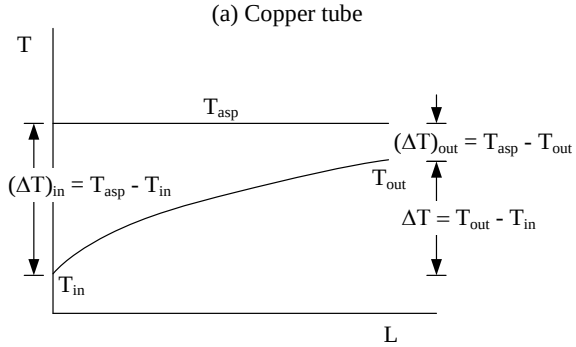

(b) Temperature profile

Figure 2. (a) Copper tube and (b) temperature profile through the collector

ANALYSIS

The present work focuses on the energy and exergy analyses of the ASWH. The energy and exergy may be expressed using the first and second laws of thermodynamics in the following ways:

Let's investigate the ASWH. On the absorber layer of the ASWH, heat balancing is based on the first law (Energy equation), and absorbed heat is dispersed by flowing water; the theoretical equation is as follows:

$$\dot{m}c_p(T_{out} - T_{in}) = A_c I_T \eta_o - \left(mc_p\right)_{asp} \frac{dT_{asp,ave}}{dt} - U_L A_c (T_{asp,ave} - T_a) \quad (1)$$

The left-hand side (LHS) of the equation represents the useable heat (1). $\dot{m}$is the water flow rate ($\dot{m} = \rho AV = \rho \dot{V}$). C_p is specific heat of water. The first term on the right-hand side (RHS) represents the heat absorbed, the second term represents the heat capacity of the ASWC, and the third term represents the total heat loss between the ASWC and the ambient. The optical efficiency (η_o) is given by Fu et al. [25]. The overall heat loss coefficient (U_L) proposed by Feng et al. [26]. $(mc_p)_{asp}$ is the mass multiply by specific heat of asphalt., The specific heat of the asphalt is given by Zhang et al. [28].

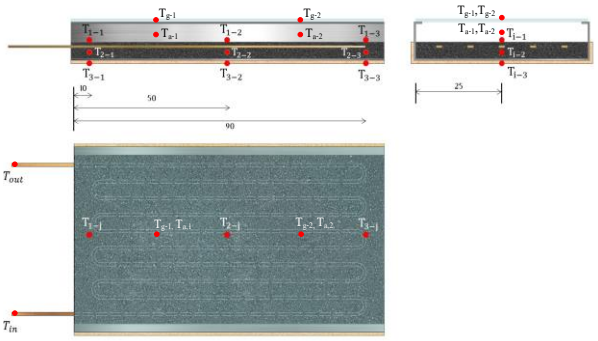

Figure 3. Measuring positions of ASWH

ASWH efficiency is the ratio of useable heat to incident solar irradiance falling on the asphalt collector surface [27].

$$\eta_I = \frac{\dot{m}c_p(T_{out}-T_{in})}{A_c I_T} \quad (2)$$

As indicated earlier, one of the aims of the study is to do an exergy analysis. Exergy is a term that expresses two principles of thermodynamics. For the analysis, the following assumptions are considered: 1. A steady-flowing process is employed. 2. Kinetic and potential energy are ignored. 3. Work transmission is disregarded. 4. Specific heat is constant. The mass balance of the water flow may be expressed in rate form as follows:

$$\sum \dot{m}_{in} = \sum \dot{m}_{out} \quad (3)$$

where is the water flow rate (kg/s) and "in" and "out" are, respectively, the entrance and outflow of the water flow. Assuming the following, the energy and exergy balances may be represented in rate form:

$$\sum \dot{E}_{in} = \sum \dot{E}_{out} \quad (4)$$

and

$$\sum \dot{E}x_{in} - \sum \dot{E}x_{out} = \sum \dot{E}x_{dest} \quad (5)$$

or

$$\sum \left(1 - \frac{T_a}{T_s}\right) \dot{Q}_s - \dot{W} + \sum \dot{m}_{in}\psi_{in} - \sum \dot{m}_{out}\psi_{out} = \dot{E}x_{dest} \quad (6)$$

with

$$\dot{Q}_s = (\tau\alpha)A_c I_T \quad (7)$$

$$\psi = (h - h_a) - T_a(s - s_a) \quad (8)$$

By substituting Equations (7) and (8) into Equation (6) as follows:

$$\sum \left(1 - \frac{T_a}{T_s}\right)(\tau\alpha)A_c I_T - \dot{m}[(h_{out} - h_{in}) - T_a(s_{out} - s_{in})] = \dot{E}x_{dest} \quad (9)$$

The first component is the rate of heat exergy, and the second term is the rate of flow-related input and output exergy. The destruction of exergy due to irreversibility is seen on the right-hand side. The ratio of net output to input exergy may be used to evaluate the exergy efficiency of an ASWH. Therefore, the efficiency of exergy may be computed as follows:

$$\eta_{II} = \frac{\dot{E}x_{out}}{\dot{E}x_{in}} = \frac{\dot{m}[(h_{out}-h_{in})-T_a(s_{out}-s_{in})]}{\left(1-\frac{T_a}{T_s}\right)(\tau\alpha)A_c I_T} \quad (10)$$

In order to compute the internal heat transfer coefficient (h_i), the useful heat in Equation (1) is to be equal the internal convection heat transfer in a copper tube as expressed in Equation (11).

$$\dot{m}c_p(T_{out} - T_{in}) = h_i A_i \Delta T_{lm} \quad (11)$$

The tube's internal surface area (A_i) and the logarithmic mean temperature difference (ΔT_{lm}) are calculated as follows:

$$A_i = \pi d_i L \quad (12)$$

and

$$\Delta T_{lm} = \frac{(T_{out}-T_{in})}{ln\left(\frac{T_s-T_{in}}{T_s-T_{out}}\right)} \quad (13)$$

The classical dimensionless of Nusselt number (Nu) inside the tube is given as:

$$Nu = \frac{h_i d_i}{k_f} \quad (14)$$

Equations (11) to (13) and Equation (14) help to calculate the Nusselt number. The Reynolds number for internal flow in a copper tube is evaluated as;

$$Re = \frac{\rho V d_i}{\mu} = \frac{4\dot{m}}{\pi d_i \mu} \quad (15)$$

The pressure loss (Δp) is a parameter to affect the irreversibility associated with flow through the tube, in other word, the exergy destruction due to friction ($\dot{E}x_{dest.f}$). The pressure loss is considered to be the total of the pressure loss caused by frictional effects and the pressure loss caused by return bends. The words for friction and slight loss are $[(fL/d_i)+\Sigma K]V^2\rho/2$, the concept of equivalent length allows us to replace the minor loss term with ($\Sigma K = fL_{eq}/d_i$).

The Δp and the $\dot{E}x_{dest.f}$ can be expressed as

$$\Delta p = \frac{f}{d_i}(L + L_{eq})\rho\frac{V^2}{2} \quad (16)$$

and

$$\dot{E}x_{dest,f} = f\frac{T_a}{T_f}\left[\frac{8\dot{m}^3}{\pi^2\rho^2 d_i^5}\right](L + L_{eq}) \quad (17)$$

where f is the friction factor that applied to the entire copper tube, d_i is the inner copper tube diameter, L_{eq} is the equivalent length. The f for circular tube can be determined from literature [29].

$$f = \frac{64}{Re} \qquad \text{Re} < 2300 \quad (18)$$

$$f = (0.790 \cdot lnRe - 1.64)^{-2} \qquad 3000 < \text{Re} < 5\times10^6 \quad (19)$$

Note that all properties in heat transfer section are to be evaluated at the mean temperature of water determined from $T_f = (T_{in}+T_{out})/2$.

EXPERIMENTAL RESULTS

In this study, the data collected for each ASWH was utilized to evaluate their performance. The research was conducted during February and March of 2022, during the daylight. As shown in Figure 4, because ambient

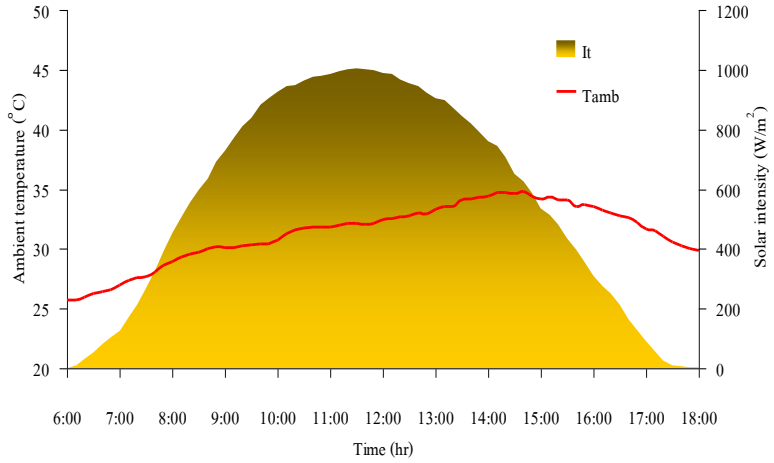

Figure 4. Variation of hourly ambient temperature and sun intensity throughout the day

temperature and sun irradiation are crucial variables for ASWH, the optimal day for displaying the ambient environment was selected.

Figure 4 illustrates the midday atmosphere. The sun intensity was zero at 6 a.m. and climbed gradually after 6:15 a.m., while the ambient temperature was around 26 degrees Celsius. Peak solar intensity and ambient temperature were around 1010 W/m^2 and 35 degrees Celsius, respectively. Due to the clear sky and absence of shadows, the solar radiation profile is unmistakably parabolic. The dimensions of the two ASWHs were identical. They were facing the same direction (15 inclination facing south). One ASWH got a water flow rate of 0.01 kg/s. While the other received 0.02 kg/s, we received. This section presents statistics from 8:00 a.m. to 4:00 p.m. during the sunny season.

Figure 5 depicts the average asphalt temperatures (T_{asp}) and the inflow water temperatures (T_{in}). Since the entering water for two ASWH was pumped from the same water tank, the T_{in} was considered to be equal. Due to the difference in water flow rate, the average asphalt temperature for, $\dot{m}$= 0.02 kg/s was between 1.5 and 4 (C lower than that for, $\dot{m}$ = 0.01 kg/s, with a range of 1.5 to 4 (C; nevertheless, the largest temperature differential between T_{asp} and Tin ((Δ)in was 30.5 (C, occurring at 12:20 pm).

Figure 6 demonstrates the difference in temperature between the exit water temperature and the intake water temperature (ΔT=T_{out} - T_{in}) for fluctuating water flow rates throughout the day. The maximum ΔT was about 17°C for $\dot{m}$ = 0.01 kg/s, and 12°C for $\dot{m}$= 0.02 kg/s, respectively. As expected, the ΔT is not more than the maximum $(\Delta T)_{in}$. As a matter of fact, the $\dot{m}$= 0.01 kg/s can approach T_{asp} than the $\dot{m}$= 0.02 kg/s. This is because a smaller flow rate may absorb more heat than a larger flow rate. Figures 5 and 6 in conjunction with Figure 2 (b) elucidate the situation.

During the testing, solar radiation was absorbed by the asphalt, some heat (useful heat) was retrieved by the feed water, some heat was lost to the environment, and the remaining heat was stored in the asphalt collector. Figure 7 depicts a comparison of accumulated heat in asphalt collectors. As noticed, the maximum cumulative heat reached 0.52 kWh and the minimum value neared 0.31

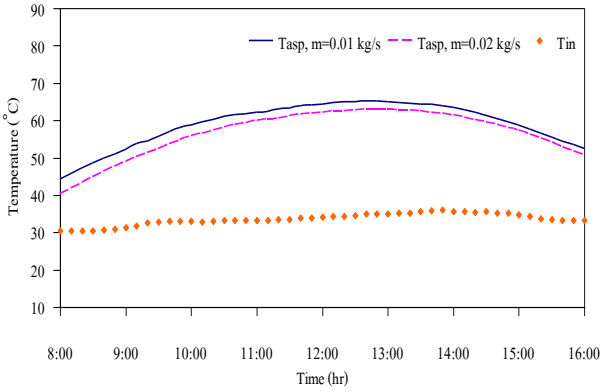

Figure 5. Variation per hour of asphalt surface temperature and intake water temperature throughout the day

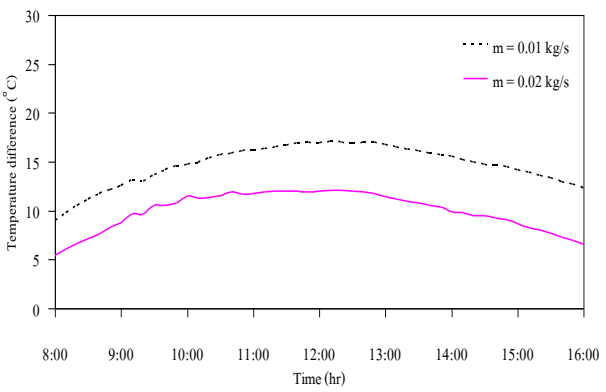

Figure 6. Hourly change of temperature disparity with respect to time of day and water flow

kWh. In contrast, the usable heat and all heat losses had a significant influence on the asphalt layer's total heat. As observed by Farzan and Zaim [27], due to the thermal inertia behavior of the asphalt collector in the ambient state, the asphalt collector is susceptible to thermal shock. From dawn until midday, asphalt may absorb and slowly release heat into the surroundings.

This section illustrates the particular enthalpy change (Δh) and the precise change in entropy (Δs) with relation to time They were informed of the energy transformation and the irreversible loss. In the case of ASWH, there is no phase shift of water flow; the specific heat may be assumed to be constant. The Δh and Δs were assessed based on the specific heat and fluid temperatures, namely the water temperatures at the input and outflow. The acquired findings were depicted in Figures 8 and 9 for $\dot{m}$= 0.01 kg/s and $\dot{m}$= 0.02 kg/s, respectively.

For $\dot{m}$ = 0.01 kg/s, the Δh and Δs varied between 37.74 to 71.6 kJ/kg and 0.122 to 0.226 kJ/kg.K respectively. Meanwhile, the Δh and $\Delta s$for $\dot{m}$= 0.02 kg/s, they were varied between 16 to 50.1 kJ/kg and 0.050 to 0.160 kJ/kg. K respectively. It is apparent that, the high $\dot{m}$ decreases the Δs whereas the low $\dot{m}$is high the Δh value.

The change in instantaneous energy efficiency is seen in Figure 10 (η_I) with time of ASWH for $\dot{m}$= 0.01 kg/s and $\dot{m}$= 0.02 kg/s. It was found that at $\dot{m}$= 0.02 kg/s is high η_I than the $\dot{m}$= 0.01 kg/s. The η_I of both ASWH were within the range 33.5 to 72% whereas the difference η_I was varied about 5 to 20%.

In addition, the immediate exergy effectiveness (η_{II}) As shown in Figure 11, It is apparent that the η_{II} has decreased than the energy efficiency which is due to the loss of irreversibility. The minimum and maximum of η_{II} were 6.0% at $\dot{m}$= 0.01 kg/s and 16.0% at $\dot{m}$= 0.02 kg/s, respectively.

The results reveal that the η_I and η_{II} are affected by water flow rate, asphalt temperature, and sun intensity. Meanwhile, the $\eta_I$and the η_{II}were increased during the late afternoon due to the cumulative heat available in absorber layer being transferred to the water flow.

In addition, the $\dot{m}$ correlated with the average internal convective heat transfer coefficient (h_i), and also the pressure loss (Δp) and the exergy destruction due to friction ($\dot{E}x_{dest.f}$). To do the data analysis, all data are determined using the relative steady-state criterion as a comparable instance reported in literature [27].

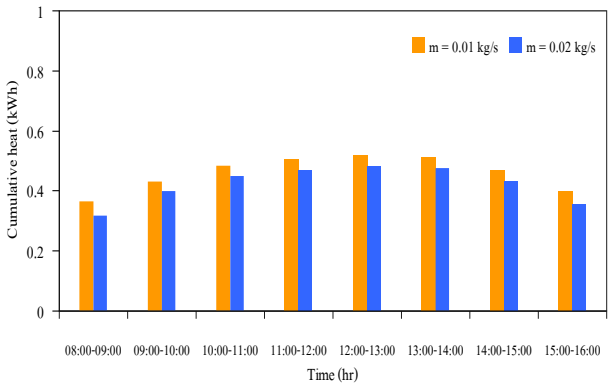

Figure 7. Variation in hourly heat accumulation based on water flow rates

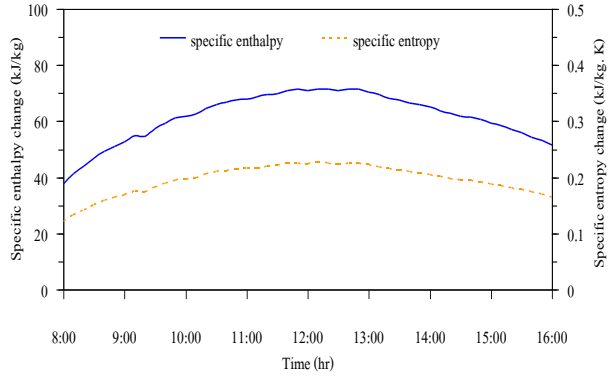

Figure 8. Variation per hour in the difference between specific enthalpy and specific entropy for, $\dot{m}$ = 0.01 kg/s

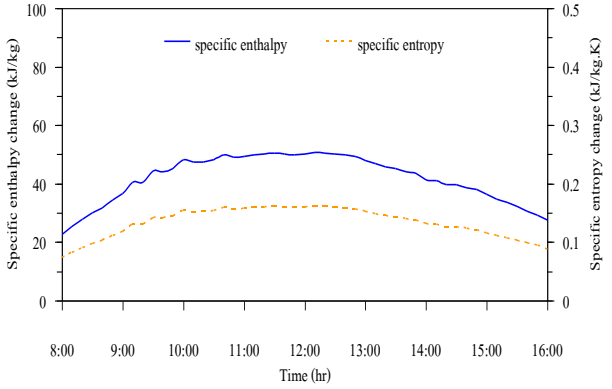

Figure 9. Variation per hour in the difference between specific enthalpy and specific entropy for, $\dot{m}$ = 0.02 kg/s

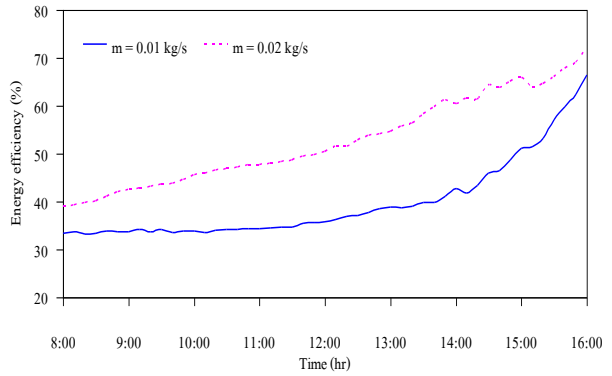

Figure 10. Energy efficiency varies hourly with time of day at various water flow rates

The copper tube seen in Figure 2 (a) is composed of a straight tube with return bends. As demonstrated in section 3, the notion of similar length was employed to determine the length equivalent of return bends to the straight tube. Figure 12 indicates the value of h_i and Nu at $\dot{m}$= 0.01 kg/s and $\dot{m}$= 0.02 kg/s. It is apparent that the value of $h_i$andNu were increased with increasing of $\dot{m}$. The maximum $h_i$andNu occur at $\dot{m}$= 0.02 kg/s, there are the values of h_i= 144.8 W/ m^2.K and Nu = 2.2. Besides this the $\dot{m}$ is a function of the Reynolds number (Re), which used to evaluate the friction factor (f) for assessment the Δp and the $\dot{E}x_{dest.f}$in the next.

Figure 13 depicts the Δp and the $\dot{E}x_{dest.f}$ at difference$\dot{m}$. The minimum of Δp and the $\dot{E}x_{dest.f}$were 432.1 Pa and 0.00423 W, respectively. Meanwhile, the maximum values were 2,355 Pa and 0.04636 W. It is apparent that, the Δp and the $\dot{E}x_{dest.f}$ were similarly increased with $h_i$andNu. The h_i,Nu, Δp and $\dot{E}x_{dest.f}$ are summarized in Table 1.

As stated in Table 1, at $\dot{m}$= 0.01 kg/s, the Re is equal 2,245, which is less than the critical Re of 2,300. The f was calculated by Equation (18). Meanwhile, at $\dot{m}$= 0.02 kg/s (Re = 4,261). The roughness (ε) of the copper tube is equal 0.0015 mm, and the inner diameter is 9.52 mm then the relative roughness (ε/d_i) is approximately 0.00016. The (ε/d_i) is closed to the smooth pipe at Re = 4,261, the f can be evaluated values reported by Yang et al. [30] as given in Equation (19). It can be seen that, the values of h_i,Nu and Δp at $\dot{m}$ = 0.02 kg/s is higher than at $\dot{m}$ = 0.01 kg/s. Similarly, the increase in the $\dot{m}$ also increases the $\dot{E}x_{dest.f}$.

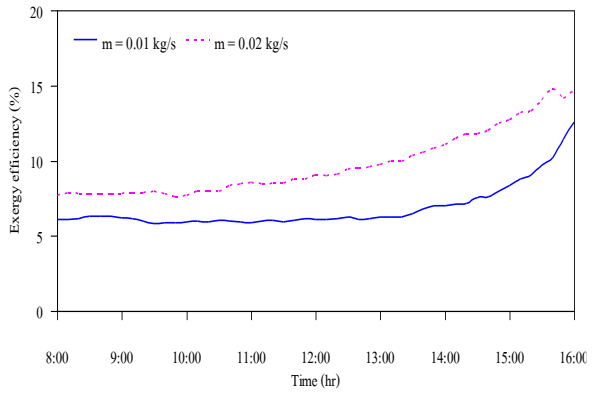

Figure 11 Variation of hourly exergy efficiency with time of day at various water flow rates.

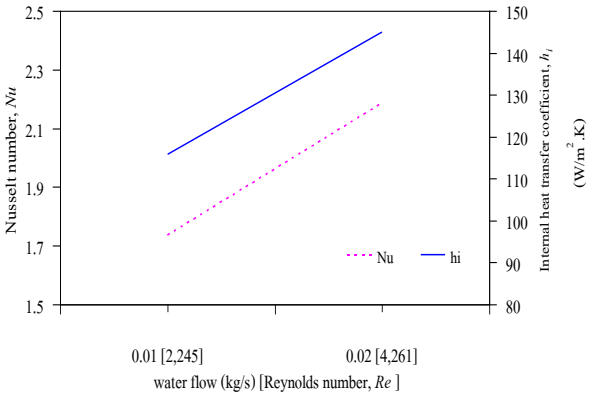

Figure 12. Variation of the Nusselt number and the internal heat transfer coefficient based on water flow

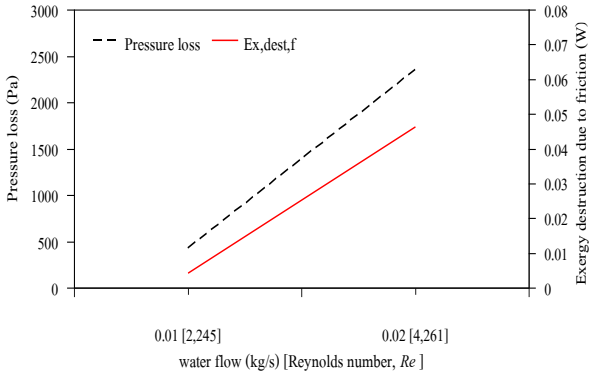

Figure 13. Variation of pressure loss and exergy degradation caused by water flow friction

Table 1. Values of Re, h_i, Nu, Δp and $\dot{E}x_{dest.f}$

Mass flow rate ($\dot{m}$)	**Reynolds number (Re)**	**Internal convective heat transfer coefficient (h_i)**	**Nusselt number (Nu)**	**Pressure loss (Δp)**	**Exergy destruction due to friction ($\dot{E}x_{dest.f}$)**
(kg/s)	(-)	(W/m^2.K)	(-)	(N/m^2)	(W)
0.01	2,245	115.8	1.74	432.1	0.00423
0.02	4,261	144.8	2.20	2,355.0	0.04636

During the data recording phase of the studies, equipment error and uncertainty may occur. Uncertainty analysis is necessary to comprehend the precision of the experiments. Farzan and Zaim [27] proposed a time-honored method for resolving uncertainty. The uncertainties arising in calculating a result (w_R) due to several independent variables is given as follows:

$$w_R = \left[\left(\frac{\partial R}{\partial x_1} w_1\right)^2 + \left(\frac{\partial R}{\partial x_2} w_2\right)^2 + \cdots + \left(\frac{\partial R}{\partial x_n} w_n\right)^2\right]^{1/2} \quad (20)$$

where the result R is a function in terms of its independent variables as x_1, x_2, x_3,……x_n, thus $R = R(x_1, x_2, x_3, \ldots, x_n)$, w_R is the uncertainty of the result, w_1, w_2,…, w_n are the uncertainties in the independent variables. This inquiry examined the water flow rate, water temperature, and other characteristics using the equipment mentioned in the experimental setup section. The uncertainty computed by Equation (21). Below is provided an illustration of the ambiguity:

$$w_{\dot{m}} = \left[\left(\frac{\partial \dot{m}}{\partial \rho}\right)^2 w_\rho^2 + \left(\frac{\partial \dot{m}}{\partial \dot{V}}\right)^2 w_{\dot{V}}^2\right]^{1/2}$$
$$\left(\frac{\partial \dot{m}}{\partial \rho}\right) = \dot{V}, \left(\frac{\partial \dot{m}}{\partial \dot{V}}\right) = \rho \quad (21)$$

After algebraic manipulation, as obtained

$$\frac{w_{\dot{m}}}{\dot{m}} = \left[\left(\frac{w_\rho}{\rho}\right)^2 + \left(\frac{w_{\dot{V}}}{\dot{V}}\right)^2\right]^{1/2} \quad (22)$$

The overall uncertainty of the measurements was found to be (about 2.0 percent for temperatures and 1.5 percent for water flow rate).

CONCLUSION

In this investigation, two asphalt solar water heaters (ASWH) were utilized and compared in a real-world environment. One ASWH was received $\dot{m}$= 0.01 kg/s while the other received $\dot{m}$= 0.02 kg/s. Between 8:00 and 16:00, both ASWH data sets were evaluated. It was established that the water flow rate, asphalt temperature, and solar intensity influence the instantaneous energy and exergy efficiency of ASWH. Due to irreversibility, the exergy efficiency of both ASWH is lower than the energy efficiency. As the intensity of the sun falls in the late afternoon, the efficiency of ASWH increases. This is because the stored heat from the absorber layer is transmitted to the water flow. In addition, the data analysis revealed the coefficient of internal convective heat transmission (h_i) and Nusselt number (Nu) increase with the water flow rate ($\dot{m}$) increases. Meanwhile, the water flow rate ($\dot{m}$) is a function of Reynolds number (Re), which used to evaluate the friction factor (f) for computed the pressure loss (Δp) and exergy destruction due to friction ($\dot{E}x_{dest.f}$). The ASWH is ideal for producing hot water because to its relatively high efficiency and cheap material costs.

REFERENCES

1. Attia, A.M.A., Nour, M., El-Seesy, A.I., and Nada, S.A., 2020. The effect of castor oil methyl ester blending ratio on the environmental and the combustion characteristics of diesel engine under standard testing conditions. *Sustainable Energy Technologies and Assessments*, 42, pp.100843. Doi: 10.1016/j.seta.2020.100843
2. Rahmanian, S., Moein-Jahromi, M., Rahmanian-Koushkaki, H., and Sopian, K., 2021. Performance investigation of inclined CPV system with composites of PCM, metal foam and nanoparticles. *Solar Energy*, 230, pp.883–901. Doi: 10.1016/J.SOLENER.2021.10.088
3. Esmaeili Shayan, M., Hayati, M.R., Najafi, G., and Esmaeili Shayan, S., 2022. The Strategy of Energy Democracy and Sustainable Development: Policymakers and Instruments. *Iranian (Iranica) Journal of Energy & Environment*, 13(2), pp.185–201. Doi: 10.5829/IJEE.2022.13.02.10
4. Esmaeili Shayan, M., Najafi, G., Ghobadian, B., and Gorjian, S., 2022. Modeling the Performance of Amorphous Silicon in Different Typologies of Curved Building-integrated Photovoltaic Conditions. *Iranian (Iranica) Journal of Energy and Environment*, 13(1), pp.87–97. Doi: 10.5829/IJEE.2022.13.01.10
5. Azadbakht, M., Esmaeilzadeh, E., and Esmaeili-Shayan, M., 2015. Energy consumption during impact cutting of canola stalk as a function of moisture content and cutting height. *Journal of the Saudi Society of Agricultural Sciences*, 14(2), pp.147–152. Doi: 10.1016/j.jssas.2013.10.002
6. Esmaeili Shayan, M., and Najafi, G., 2019. Energy-Economic Optimization of Thin Layer Photovoltaic on Domes and Cylindrical Towers. *International Journal of Smart Grid - ijSmartGrid*, 3(2), pp.84–91. Doi: https://doi.org/10.20508/ijsmartgrid.v3i2.61.g57
7. Esmaeili Shayan, M., Najafi, G., Ghobadian, B., Gorjian, S., and Mazlan, M., 2022. A novel approach of synchronization of the sustainable grid with an intelligent local hybrid renewable energy control. *International Journal of Energy and Environmental Engineering*, pp.1–12. Doi: 10.1007/S40095-022-00503-7
8. Ghasemzadeh, F., Esmaeilzadeh, M., and Esmaeili shayan, M., 2020. Photovoltaic Temperature Challenges and Bismuthene Monolayer Properties. *International Journal of Smart Grid*, 4(4), pp.190–195. Doi: https://doi.org/10.20508/ijsmartgrid.v4i4.131.g109
9. Esmaeili Shayan, M., Najafi, G., Ghobadian, B., Gorjian, S., Mazlan, M., Samami, M., and Shabanzadeh, A., 2022. Flexible Photovoltaic System on Non-Conventional Surfaces: A Techno-Economic Analysis. *Sustainability*, 14(6), pp.3566. Doi: 10.3390/SU14063566
10. Esmaeili Shayan, M., 2020. Solar Energy and Its Purpose in Net-Zero Energy Building. In: Pérez-Fargallo A, Oropeza-Perez I (eds) Zero-Energy Buildings - New Approaches and Technologies. IntechOpen.
11. Azadbakht, M., Shayan, M.E., and Jafari, H., 2013. Investigation of Long Shaft Failure in John Deere 955 Grain Combine Harvester under Static Load. *Universal Journal of Agricultural Research*, 1(3), pp.70–73. Doi: 10.13189/UJAR.2013.010305
12. Esmaeili Shayan, M., and Ghasemzadeh, F., 2020. Nuclear Power Plant or Solar Power Plant. In: Awwad N (ed) Nuclear Power Plants - The Processes from the Cradle to the Grave. IntechOpen, Landon.
13. Esmaeili Shayan, M., Najafi, G. and Nazari, A., 2021. The Biomass Supply Chain Network AutoRegressive Moving Average Algorithm. *International Journal of Smart Grid*, 5(1), pp.15-22 Doi: 10.20508/IJSMARTGRID.V5I1.153.G135
14. Ghasemzadeh, F., and Esmaeili Shayan, M., 2020. Nanotechnology in the Service of Solar Energy Systems. In: Nanotechnology and the Environment. IntechOpen, London.
15. Esmaeili Shayan, M., and Hojati, J., 2021. Floating Solar Power Plants: A Way to Improve Environmental and Operational Flexibility. *Iranian (Iranica) Journal of Energy & Environment*, (4), pp.337–348. Doi: 10.5829/IJEE.2021.12.04.07
16. Esmaeili Shayan, M., Najafi, G., and Banakar, A., 2017. Design, Fabrication and Techno-Economic Analysis of Solar Energy Conversion System Based on Flexible Solar Panels. In: EU PVSEC 2017 – 33rd European PV Solar Energy Conference and Exhibition. Amsterdam.
17. Esmaeili Shayan, M., Esmaeili Shayan, S., and Nazari, A., 2021. Possibility of supplying energy to border villages by solar energy sources. *Energy Equipment and Systems*, 9(3), pp.279–289. Doi: 10.22059/EES.2021.246079
18. Esameili Shayan, M., Najafi, G., and Esameili shayan, S., 2021. Design of an Integrated Photovoltaic Site: Case of Isfahan's Jarghouyeh photovoltaic plant (In Persian). *Journal of Energy Planning And Policy Research*, 6(4), pp.229–250.
19. Esmaeili shayan, M., Najafi, G., and Banakar, A. ahmad, 2017. Power Quality in Flexible Photovoltaic System on Curved Surfaces. *Journal of Energy Planning And Policy Research*, 3(17), pp.105–136.

20. Esmaeili Shayan, M., Najafi, G., and Lorenzini, G., 2022. Phase change material mixed with chloride salt graphite foam infiltration for latent heat storage applications at higher temperatures and pressures. *International Journal of Energy and Environmental Engineering*, pp.1–11. Doi: 10.1007/S40095-021-00462-5
21. Walker, A., 2013. Solar Energy : Technologies and Project Delivery for Buildings. Wiley.
22. Shayan, M.E., Najafi, G., Ghobadian, B., Gorjian, S., and Mazlan, M., 2022. Sustainable Design of a Near-Zero-Emissions Building Assisted by a Smart Hybrid Renewable Microgrid. *International Journal of Renewable Energy Development*, 11(2), pp.471–480. Doi: 10.14710/IJRED.2022.43838
23. Esmaeili Shayan, M., Najafi, G., and Ghasemzadeh, F., 2020. Advanced Study of the Parabolic Trough Collector Using Aluminum (III) Oxide Seal. *International Journal of Smart Grid - ijSmartGrid*, 4(3), pp.111–116. Doi: https://doi.org/10.20508/ijsmartgrid.v4i3.108.g98
24. Azadbakht, M., Shayan, M.E., Jafari, H., Ghajarjazi, E., and Kiapei, A., 2015. Factor Resistance Comparison of a Long Shaft in 955 and 1055 John Deere Grain Combine. Doi: 10.5281/ZENODO.1100909
25. Fu, X., Li, D., Wang, H., Yang, J., and Wei, X., 2022. Multi-objective optimization of guide vane closure scheme in clean pumped-storage power plant with emphasis on pressure fluctuations. *Journal of Energy Storage*, 55, pp.105493. Doi: 10.1016/J.EST.2022.105493
26. Feng, L., Zhang, X., Li, C., Li, X., Li, B., Ding, J., Zhang, C., Qiu, H., Xu, Y., and Chen, H., 2022. Optimization analysis of energy storage application based on electricity price arbitrage and ancillary services. *Journal of Energy Storage*, 55, pp.105508. Doi: 10.1016/J.EST.2022.105508
27. Farzan, H., and Zaim, E.H., 2021. Feasibility study on using asphalt pavements as heat absorbers and sensible heat storage materials in solar air heaters: An experimental study. *Journal of Energy Storage*, 44, pp.103383. Doi: 10.1016/J.EST.2021.103383
28. Zhang, L., Yu, H., Wang, W., Xie, H., Wang, M., Yang, S., Chen, S., and Liu, X., 2022. Revealing the lithium dendrite deposition/dissolution progression based on Monte Carlo method. *Journal of Energy Storage*, 55, pp.105473. Doi: 10.1016/J.EST.2022.105473
29. Çengel, Y.A., and Boles, M.A., 2008. Thermodynamics : an engineering approach. McGraw-Hill Higher Education.
30. Yang, M., Zhang, X., Zhou, X., Liu, B., Wang, X., and Lin, X., 2021. Research and Exploration of Phase Change Materials on Solar Pavement and Asphalt Pavement: A review. *Journal of Energy Storage*, 35, pp.102246. Doi: 10.1016/J.EST.2021.102246

Persian Abstract

چکیده

با داشتن کیلومترها جاده آسفالته، با این حال با هدر رفتن این گرما، در این تحقیق تلاش شده است تا گرمای انرژی تجدیدپذیر جاده استخراج شود. هدف از این آزمایش مقایسه بازده انرژی و اگزرژی مواد مختلف آبگرمکن‌های خورشیدی آسفالتی (ASWH) و همچنین انتقال گرما از طریق لوله آب و چگونگی تأثیر اصطکاک بر تخریب اکسرژی است. سرعت جریان آب یک ASWH 0.01 کیلوگرم بر ثانیه بود، در حالی که جریان آب دیگری ۰/۰۲ کیلوگرم بر ثانیه بود. هر ASWH 0.5 متر مربع مساحت دارد. لوله مسی به عمق ۱۰ میلی‌متر در آسفالت مدفون شده است. ۱۵ درجه زاویه میل است. نتایج نشان می‌دهد که راندمان انرژی و اگزرژی برای سرعت جریان آب ۰/۰۲ کیلوگرم بر ثانیه به طور منطقی بالا است. بسته به سرعت جریان آب، دمای آسفالت و شدت نور خورشید، بازده انرژی و اگزرژی به ترتیب از ۳۲٪ به ۶۵٪ و ۵/۸٪ به ۱۶٪ تغییر کرد. نرخ جریان آب یک پارامتر ضروری برای تخمین ضریب انتقال حرارت همرفتی داخلی و عدد رینولدز به منظور محاسبه ضریب اصطکاک در لوله مسی بر اساس انتقال حرارت جابجایی داخلی است. در مقابل، ضریب اصطکاک نتیجه افت فشار و تخریب اکسرژی ناشی از اصطکاک است.